Numerical investigation of pulsed flow in aortic aneurism with and without stent by lattice Boltzmann method

Farouk Mezali, Saâdia Benmamar, Mohamed Saber Hamouda, and Mohamed Aghiles Zakaria Mezali

Abstract− Endovascular treatment of aortic aneurysms with an endoprosthesis is proposed for the prevention of the aneurysms' rupture risk and clogging of blood vessels. This paper aims to study the impact of stents with different porosities, placed in fusiform aortic aneurysms, on the hemodynamic parameters: velocity and shear rate of the flow inside the aneurysms, using pulsed boundary conditions derived from real measurements. The numerical investigations are performed with the Lattice Boltzmann method. The blood is treated as a Newtonian fluid and then as a non-Newtonian fluid with the Carreau-Yasuda and Cross models. The reduction obtained by a single stent is modest and unfavorable to thrombotic occlusion. Overlapping of several stents is proposed to promote occlusion. The results found show good agreement with medical theory.

***Keywords*− Lattice Boltzmann, Fusiform aortic aneurysm, stent, pulsed flow, Computational Fluid Dynamics.**

I. Introduction

Cardiovascular diseases represent the leading cause of mortality worldwide. They are responsible for 36 million deaths annually and almost 70% of total deaths worldwide [1]. Among these diseases are aneurysms.

An aneurysm is a vascular disorder related to the wall weakening of a vessel, resulting in a small sac of various shapes (fusiform, saccular). Under some conditions, the wall of this sac or aneurysm may rupture and become harmful, even fatal [2, 3]. There are two techniques for treating it: surgical, which consists of carrying out an operation on the patient to directly approach the aneurysmal zone and replace it with a synthetic tube called a prosthesis, and other surgical forms, such as clipping, coating, etc[4, 5].

The second technique is endovascular treatment, which involves inserting a stent (an endoprosthesis) inside the aneurysmal aorta through the femoral arteries. The endovascular stent graft technique is mainly used for the treatment of abdominal aortic aneurysms (AAAs). Stent graft techniques have the advantage of being minimally invasive and present a lower risk of mortality and complications than surgery in the short term. On the other hand, it has the disadvantage of producing poorer results over the long term and necessitating lifetime monitoring [3].

Manuscript received September 28, 2022, revised March 27, 2023.

F. Mezali is with LRS-EAU Laboratory, Ecole Nationale Polytechnique, Algiers, ALGERIA and Hydraulic Department, University Mohamed Boudiaf Of M'sila, ALGERIA (e-mail: mezali_farouk@yahoo.fr).

S. Benmamar is with the Hydraulic Department, LRS-EAU Laboratory, Ecole Nationale Polytechnique, Algiers, ALGERIA (e-mail: saida.benmamar@g.enp.edu.dz).

M. S. HAMOUDA is with SEAAL (Société des Eaux et de l'Assainissement d'Alger), ALGERIA (e-mail : hamouda.mohamed.saber@gmail.com)

M. A. Z. Mezal is with SEAAL (Société des Eaux et de l'Assainissement d'Alger), ALGERIA (e-mail : zakiaghiles@gmail.com)

Digital Object Identifier (DOI): 10.53907/enpesj.v3i2.139

Flow diverter stents are relatively new techniques in the treatment of aneurysms, particularly intracranial aneurysms. However, this technique is sometimes used in the treatment of aortic aneurysms. Regarding the aneurysm's volume reduction and thrombosis, as well as the patency of the lateral branches and the prevention of rupture, it has demonstrated satisfactory results. These results must be investigated further, to provide more complete and extensive guidance [6].

This kind of aneurysm is also treated by the uncovered stent. The common basic idea behind these last two techniques is the reduction of blood flow in the aneurysmal sac to stabilize it and, therefore, reduce the risk of its rupture [7].

This work is devoted to understanding and evaluating the hemodynamics of abdominal aortic aneurysm (AAA) with and without stents through a hemodynamic analysis carried out using the Lattice Boltzmann method (LBM). To reach this goal, the real pulsating flow is used as boundary condition input. The basic idea behind the LBM is to use discrete velocity models to obtain an approximate solution for an incompressible Navier Stokes [8, 9]. Non-Newtonian behavior is taken into account in the flow modeling through the Carreau-Yasuda and Cross models. Two types of analysis are carried out: qualitative and quantitative. The qualitative analysis is made on the shape and form of the results based on the velocity and the shear rate. Quantitative analysis is performed on "velocity" and "shear rate" within the aneurysm sac before and after stent placement.

II. Lattice-Boltzmann (LB) model

In this paragraph, the main aspects of the used model are explained. The fluid is represented by the lattice-Bhatnagar-Gross-Krook model (LBGK). This model is defined by the propagation-collision equation as follows:

$$f_i(r + \Delta t\, v_i, t + \Delta t) = \left(\frac{1}{\tau}\right) f_i^0(r,t)\left(1 - \left(\frac{1}{\tau}\right)\right) \quad (1)$$

Where $f_i(r,t)$ is the probability distribution function. This function gives the probability that a fluid particle of velocity $\boldsymbol{v_i}$ enters at the point of coordinate r of the lattice at time t. The probable allowable velocity $\boldsymbol{v_i}$ depends on the lattice structure. In our case, one thing a cell of the type D2Q9 (Fig.1).

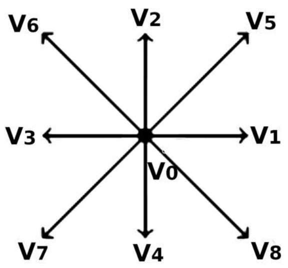

Fig. 1: Discrete velocities of the D2Q9 lattice model.

The index i varies from 0 to 8, where 8 is the number of lattice link. By convention $v_0 = 0$, and f_0 represents the distribution of particle density at rest.

The density and velocity of the fluid at the macroscopic scale are given as follows:

$$\rho = \sum_{i=0}^{8} m_i f_i \tag{2}$$

$$\rho \boldsymbol{u} = \sum_{i=0}^{8} m_i f_i \boldsymbol{v_i} \tag{3}$$

The time step *Δt of the simulation* is taken equal to 1 [9-11]. The number τ is the relaxation time and $f_i^{(0)}$ are the functions of local equilibrium. Their expressions are:

$$f_i^{(0)} = \rho \frac{C_4}{C_2}\left(1 + \frac{v_{i\alpha}u_\alpha}{c_s^2} + \frac{1}{2}\left(\frac{v_{i\alpha}u_\alpha}{c_s^2}\right)^2 - \frac{u^2}{2c_s^2}\right), \tag{4}$$

$$f_0^{(0)} = \rho\left(1 - \frac{C_0 C_4}{C_2^2}\right)\left(1 - \frac{u^2}{2c_s^2}\right)$$

Generally, the square speed of sound is chosen like $c_s^2 = v_l^2\left(\frac{C_4}{C_2}\right)$ where $v_l = \frac{\Delta x}{\Delta t}$.

The quantities m_i are the lattice weight, their values are associated with the lattice directions and depend on its dimension: $m_{1-4} = \frac{1}{9}$ and $m_{5-8} = \frac{1}{36}$.

C_0, C_2 and C_4 are constants and depend on the structure of the lattice. All these constants, follow from the isotropy condition [11, 12]. In the case of D2Q9, they are equal to: $C_0 = 20$, $C_2 = 12$, $C_4 = 4$.

One can show that the equation (1), which represents the dynamics of fluid particles on the microscopic scale, can reproduce the Navier-Stokes and continuity equations [9-11]:

$$\begin{gathered} \partial_t \rho + \rho \nabla \cdot u = 0 \\ \partial_t u + u \cdot \nabla u = -\nabla p + \nu \nabla^2 u \end{gathered} \tag{5}$$

The pressure is related to the density by $p = c_s^2 \rho$. The cinematic viscosity, expressed in lattice units, is written

$$\nu = \Delta t v_l^2 \frac{C_4}{C_2}\left(\tau - \frac{1}{2}\right)$$

In D2Q9 case , the speed of sound becomes $c_s = \frac{1}{\sqrt{3}} v_l$ and the viscosity

$$\nu = \frac{1}{3}\left(\tau - \frac{1}{2}\right) v_l^2 \Delta t. \tag{6}$$

Previous macroscopic variables (u, p, ν), given by equations of lattice Boltzmann, are in lattice unit (lu). The conversion to physical units is given by a simple transformation: $u_p = \frac{\delta x}{\delta t} u_{lb}$, $\nu_p = \frac{\delta x^2}{\delta t} \nu_{lb}$ where δx and δt are the space step and the time step respectively.

A. Boundary conditions to the limits

1. Dirichlet condition at the inlet

A Dirichlet boundary condition is posed at the inlet aorta artery, and a subroutine has been introduced inside the elaborate computer code to make the velocity variable at the inlet.

The realization of the Dirichlet condition is carried out by Zou and He condition [13]. In fact, this condition extends the bounce-back conditions to the non-equilibrium part $f_i^{neq} = f_i - f_i^{eq}$ of the distribution function f_i. For Dirichlet boundary condition, the values that the solution (velocity or density) must verify on the solid or fluid boundaries are specified, and subsequently the missing

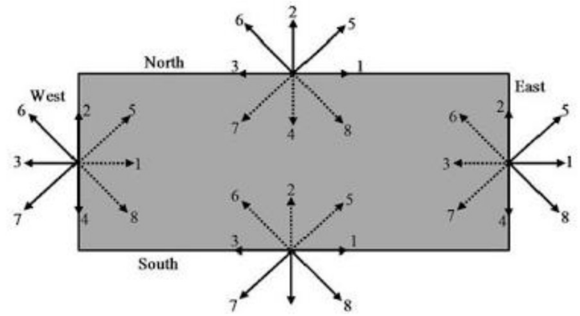

Fig. 2: The East, West, North and South boundaries for the Dirichlet condition.

Consider the case of fluid entering a channel on its western side, as shown in fig. 2. u_x and u_y are specified. Following the propagation phase, the distribution functions $f_0, f_2, f_3, f_4, f_6, f_7$ for the D2Q9 model are known. It is still unknown ρ and f_1, f_5, f_8 which are given by:

$$\rho = \frac{1}{1-u}\left(f_0 + f_2 + f_4 + 2(f_3 + f_6 + f_7)\right)$$

$$f_1 = f_3 + \frac{2}{3}\rho u$$

$$f_5 = f_{\grave{e}} - \frac{1}{2}(f_2 - f_4) + \frac{1}{2}\rho v$$

$$f_8 = f_6 + \frac{1}{2}(f_2 - f_4) - \frac{1}{2}\rho v + \frac{1}{6}\rho u$$

It is to highlight that by setting the velocity to zero $(u = v = 0)$, the conditions of Zou and He are reduced to a simple bounce-back.

2. Wall Conditions (Bounce-Back)

Bounce-back boundary conditions are most often used for straight or non-straight solid walls to achieve the no-slip condition. They are widely used in the simulation of fluid flows with complex geometries. The principle is that when a fluid particle hits a solid wall, its momentum is reversed, in other words, the particle bounces in the opposite direction of its motion (Fig. 2), the mathematical expression which expresses this occurrence is:

$$f_{\bar{i}}^{out}(x_b, t + \Delta t) = f_i^{in}(x_b, t) \tag{7}$$

where $f_{\bar{i}}^{out}$ denotes the outgoing distribution functions of the solid wall. While f_i^{in} expresses the incoming distribution functions.

The bounce-back condition can be coded by two ways: either all distributions are reflected, or only outgoing distributions are swapped out for their geometric opposites.

The reflection of all the distributions makes it possible to ensure that the adhesion condition is obtained regardless of the geometric configuration. Thus, the code has only one subroutine for all zero-velocity boundaries [14]. In this work, this option was adopted.

3. Outlet boundary conditions

The normal gradient of the distribution functions at the output boundary is zero. After propagation, the unknowns distributions f_3, $f_6$and $f_7$are calculated simply : $f_a(Nx, j) = f_a(N_{x-1}, j), (a = 3,6,7 ; j = 1, N_y)$, where $N_x$and $N_y$are the numbers of the cells meshes in the x and y direction respectively.

B. Initial conditions

One imposes initial velocity macroscopic quantities $u_0 = 0$, which are used to calculate the distributions functions $f_i^0(x, u_0, t = 0)$, which are used in their turns as initial conditions for f_i: $f_i = f_i^0$.

III. Non-Newtonian blood viscosity models

Tu and Deville [15] found that the rheological properties of blood can significantly affect flow phenomena.
For our case study, O'Callaghan [16] showed that in areas of slow flow such as aneurysms and recirculation zones, where blood stagnates for a significant time period, the non-Newtonian nature of blood is important.
For Newtonian fluids, the stress tensor follows Newton's law for viscosity, expressing a linear and explicit stress-strain rate by the relation:

$$\sigma = \mu\dot{\gamma} \tag{8}$$

With,
σ: the shear stress tensor Pa.
$\dot{\gamma}$: is the shear rate tensor s-1.
μ: Newtonian dynamic viscosity, equal to 0.0035 Pa.s.
For non-Newtonian fluids, the dynamic viscosity is a function of the shear rate. The stress tensor is expressed by the relation:

$$\sigma = \mu(\dot{\gamma})\dot{\gamma}$$

Where $\dot{\gamma} = \sqrt{2\, S_{\alpha\beta} S_{\alpha\beta}}$is the module of the strain rate tensor with $S_{\alpha\beta} = 1/2\left(\partial_\beta u_\alpha + \partial_\alpha u_\beta\right)$

The tensor $S_{\alpha\beta}$ can be calculated locally without passing through the operations of derivation, such as:

$$S_{\alpha\beta} = -\frac{1}{2\rho\tau\Delta t}\frac{C_2}{C_1}\sum_i v_{i\alpha} v_{i\beta}\left(f_i - f_i^{(0)}\right) \tag{9}$$

In this study, it's proposed to make a comparison between the Carreau-Yasuda model, the Cross model, and the Newtonian model. The last model is taken as the reference. The two models that are used for modeling the non-Newtonian behavior of blood are presented below. There are different models that allow characterization of the behavior of non-Newtonian fluids. They sometimes make it possible to highlight threshold stress, shear-thickening, or shear-thinning behavior. The description given here avoids the molecular mechanisms which govern these laws.

A. Carreau-Yasuda model

In Carreau-type models (Cross, Carreau-Yasuda, Cross), λ is the relaxation time constant with the unit of second. Dynamic viscosity for C-Y model is given by

$$\mu = \mu_\infty + \frac{\mu_0 - \mu_\infty}{(1 + (\lambda\dot{\gamma})^a)^{\frac{a}{n-1}}} \tag{10}$$

With $\mu_0 = 0.16\ Pa.s, \mu_\infty = 0.0035\ Pa.s\ \lambda = 8.2s, n = 0.2128, a = 0.64$ [17].
At high shear rates, well above $100\, s^{-1}$, the viscosity of Carreau's model is very close to that of Newton. The Carreau-Yasuda model is the type of the Carreau model that tends to Newtonian rheology at low shear rates.

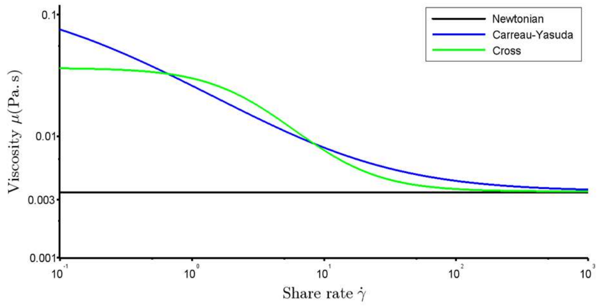

Fig.3: Log-log plot of C-Y, Cross and Newtonien model viscosity.

B. Cross model

Also known as the Bird-Carreau model, is the simplified form of the Carreau model, which may be a good candidate for modeling blood flow in large arteries due to the shorter viscosity range generated by the model [17].

$$\mu = \mu_\infty + \frac{\mu_0 - \mu_\infty}{1 + (\lambda\dot{\gamma})^a} \tag{11}$$

With $\mu_0 = 0.0364\ Pa.s, \mu_\infty = 0.0035\ Pa.s\ \lambda = 0.38s$, $a = 1.45$. The fig. 3 presents the plot of dynamic viscosity versus shear rate for the three models in a log-log scale reference.

IV. Simulation parameters

A. Geometric parameters

The case of fusiform abdominal aortic aneurysm (AAA) is treated in this section (Fig. 4). The geometry and dimensions are taken from a real image of an AAA [18]**.** This aneurysm is shown in fig. 5.

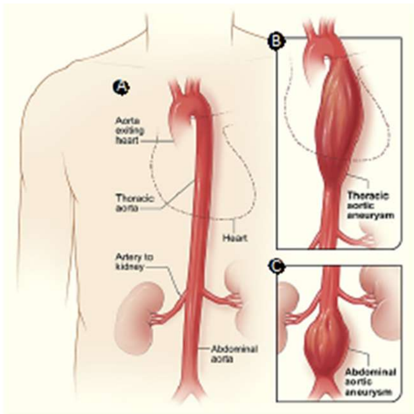

Fig. 4: A: Normal aorta, B: Thoracic aortic aneurysm, C: Abdominal aortic aneurysm [19].

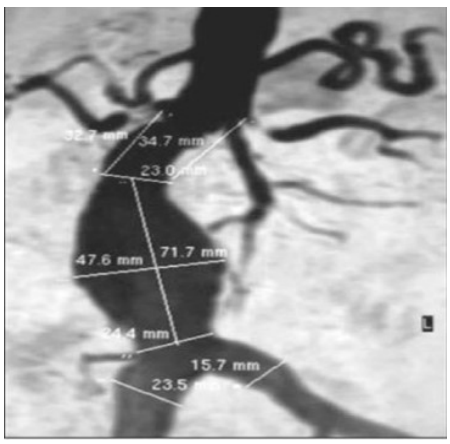

Fig. 5: Abdominal aortic aneurysm [18].

The characteristics of this aneurysm are:
Length l = 71.7mm, height h = 47.6mm, vessel length L = 126mm, inlet diameter D_e =23mm, outlet diameter D_s =24.4mm.
Due to the complexity of arterial geometry, an ideal simplified geometry has been used to represent the actual geometry above. The geometry size of our simulation model is 274 × 120 (lattice unit), with a channel width of 274 (lattice unit).
The AAA geometry used is shown in fig. 6 below and their dimensions (in lattice) are detailed in table I.
Due to the dimensions of aneurysms, two types of stent are used, one with 4 struts and the other with 6 struts. A strut is set of metal parts that form the stent, separated from each other by spaces. The struts used in simulations have a square shape, length l_s= 40 (lattice unit) and thickness e_s= 4 (lattice unit) for the case of stent with 4 struts. And for case of the stent of 6 struts, a length is l_s =25 (lattice unit), thickness e_s= 4 (lattice unit). The parameters of the stents used for each case are shown in table II.

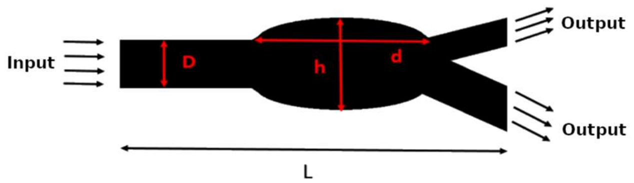

Fig. 6: Simplified geometry of the abdominal aorta

Table. I

Abdominal aortic aneurysm dimensions in (lu)

Aneurysm Parameters	D	d	h	L
Size (lu)	93	311	184	274

Table. II

Parameters of the stents for the simulation.

	Parameters(lu)		
Stent type	l_s	*Espacement*	*Porosité %*
4 struts	40	44	50
6 struts	25	38	61

The porosity was calculated with the following relationship:

$$P = \frac{d - (n * l_s)}{d}$$

With :
P: porosity;
d: the aneurysm's length (lu);
l_s : the strut's width (lu);
n: strut's number (lu).
The three geometries used in the simulations are shown below:

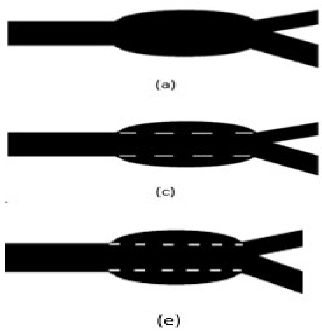

Fig. 7: AAA without stent b) AAA with 4-strut stent- c) AAA with 6-strut stent.

B. Flow Parameters

To render the simulation more realistic, a pulsating flow is used, and therefore the effect of heartbeats is no longer neglected. The elasticity of the wall is not taken into account. The average of one heartbeat cycle was taken as 0.8 seconds since the contraction phase of the heart (systole) lasts about 0.25 seconds. The relaxation phase (filling phase) is called diastole. Its duration is about 0.55 seconds, so the sum of the two phases is 0.8 seconds.
To fit the pulse velocity into our code, the blood flow rate graphs corresponding to the study area (the aorta) are taken from a real experiment, as shown in fig. 8 and 9 below. Then, dividing by the surface, the desired velocity graph is obtained.

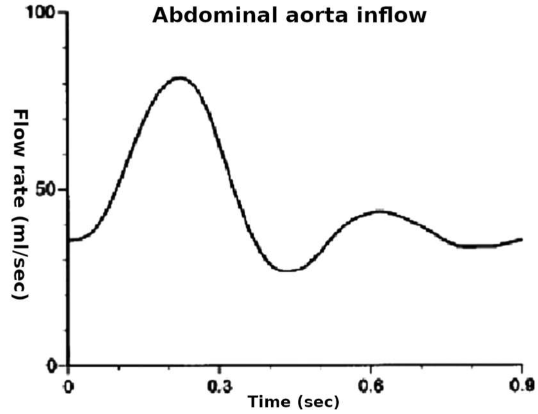

Fig.8: Blood flow in the abdominal aorta [20].

After this step, we used the Origin software to find the speed functions which are of polynomial type of the tenth degree after we provided the maximum points of the graphs of real speeds. The approximate mathematical function of blood velocity is:

$$\begin{aligned} \boldsymbol{V(t)} = {} & 0.091 + 0.013\,t - 1.191\,t^2 + 53.981\,t^3 \\ & + 115.608\,t^4 - 3959.907\,t^5 \\ & + 19484.015\,t^6 - 44659.211\,t^7 \\ & + 54599.737\,t^8 - 34553.635\,t^9 \\ & + 8929.843\,t^{10} \end{aligned}$$

This function is valid for a time less than 0.8s, so it had to be made periodic with a period of 0.8s.

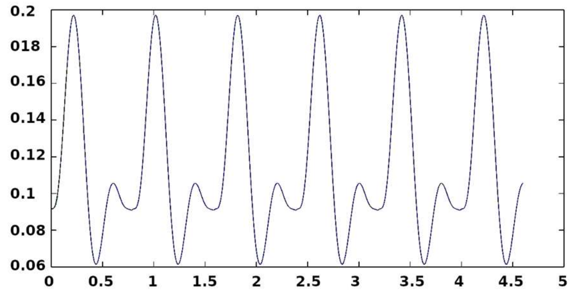

Fig. 9: Periodic pulse velocity curve in the abdominal aorta.

For blood rheology, blood is treated as a Newtonian fluid and also as a non-Newtonian fluid by assuming that the viscosity is constant concerning the shear rate in the case of Newtonian behavior. For the case of non-Newtonian behavior of blood, the equations (10)-(11) of Cross and Carreau-Yasuda are used to model blood flow.

I. RESULTS AND DISCUSSIONS

In this section, the results of the simulations obtained by the developed code are presented. First, a qualitative analysis of the velocity and shear rate of the blood is made, followed by a quantitative analysis of the systolic and diastolic velocity generated by the heart.

The visualization of the results is carried out by the free software ParaView, which is created from the VTK libraries (Visualization Tool Kit). The software is cross-platform and intended for scientific and interactive data visualization.
Then, to confirm our results, we compared them to the results provided by the reference software in the Computational fluid dynamics (CFD) field "Ansys Fluent". Blood flow in the abdominal aorta is calculated from the Navier-Stokes equations (5) solved using Fluent 19.0 by the finite volume method. In this simulation, the blood is considered as a Newtonian fluid with a viscosity of $0.003\ Pa.s$ and a density of $1060\ kg/cm^3$. As Fluent does not deal with variable velocities boundary conditions directly, it was necessary to write an algorithm in the C++ language that contains the velocity equations and introduce them into the initial conditions before launching the simulation.

A. Comparison with ANSYS-FLUENT results

In this part, the analyze of the results of two simulations is performed. The first is done using the elaborate LBM code. The second simulation is made with the commercial software ANSYS-FLUENT based on the Navier-Stokes equations (5) solved by the finite volume method. This simulation allowed us to validate our model by comparing our results with the results of ANSYS-FLUENT.

A qualitative analysis of the two simulations is performed by introducing the same input conditions. From the comparison of the results in fig. 10 above, it's shown that the distribution of the velocity is similar in both solvers, with a small difference inside the aneurysm, which shows that they are in acceptable agreement.

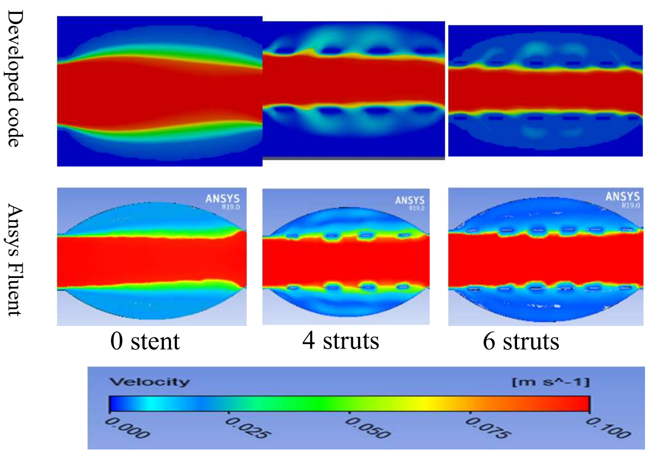

Fig. 10: The comparison between Flow velocity for the two solvers: developed code and ANSYS for fusiform aneurysm.

B. Qualitative analysis

The qualitative analysis is made based on the study of the variation of the velocity and the shear rate for the two studies' cases.

1. Velocity field: systolic

The relatively high velocities are found at the entrance and exit of the aneurysm. And the lowest velocity is observed at the level of the aneurysmal sac.
A comparison between the different models in the case of systolic velocity is given in fig.11. It is the greatest velocity that crosses the abdominal aorta.

Table III contains the maximum velocity values obtained inside the sacs for the three rheological models.

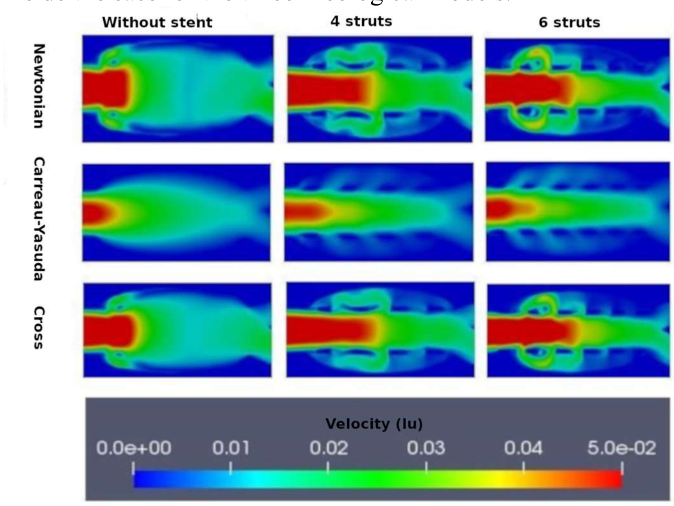

Fig. 11: Representation of the velocity field with different porosities for the three rheological models (systolic velocity)

Table. III

Maximum values of the velocity (lu) obtained in the control line (inside the sacs) for the three rheological models

	0 stent	4 struts	6 struts
Newt	0.0173	0.0138	0.0126
C-Y	0.0142	0.0118	0.0109
Cross	0.0166	0.0131	0.0119

Newtonian model

The maximum velocity is around 0.0173 (lu) for aneurysm without a stent, it decreases afterward to 0.0138 (lu) in the model with four struts and also decreases to reach the value of 0.0126 (lu) for the six struts model, this is due to the decrease in porosity caused by the stent struts at the aneurysm entrance.

Carreau-Yasuda model

This model is different from the other models, the only similar thing is that we have a reduction in the velocity obtained inside the aneurysmal sacs after the placement of a stent. The maximum velocity in the control line inside the sacs decreases from 0.0142 (lu) in the without stent model to 0.0109 (lu) in the six-strut model.

Cross model

The same interpretation is made as that on the Newtonian model. Velocity decreases in aneurysmal sacs after the placement of a stent in the aneurysm. The maximum velocity for this model decreases from 0.0166 (lu) for the aneurysm without a stent until reaching a value of 0.0119 (lu) in the aneurysm with six struts. These values are smaller than those recorded in the Newtonian model.

Velocity in the middle of the artery

To see the influence of the location of the stents on the flow, we checked the velocities in the middle of the artery for the three rheological models (

Table. IV).

Table. IV

Maximum velocity values (lu) obtained in the middle of the stent for the 3 rheological models

	0 stent	4 struts	6 struts
Newt	0.04889	0.0687	0.0864
C-Y	0.0381	0.0562	0.0627
Cross	0.0467	0.0651	0.0783

After visualizing the flow of the three models with and without a stent, we notice a significant increase in flow velocity after the placement of a stent, more specifically in the middle of the stent, indicating that the stent placement promotes flow toward the fusiform aneurysm's outlet.

2. Velocity field: diastolic

The velocity results for the smallest velocity in the abdominal aorta is presented

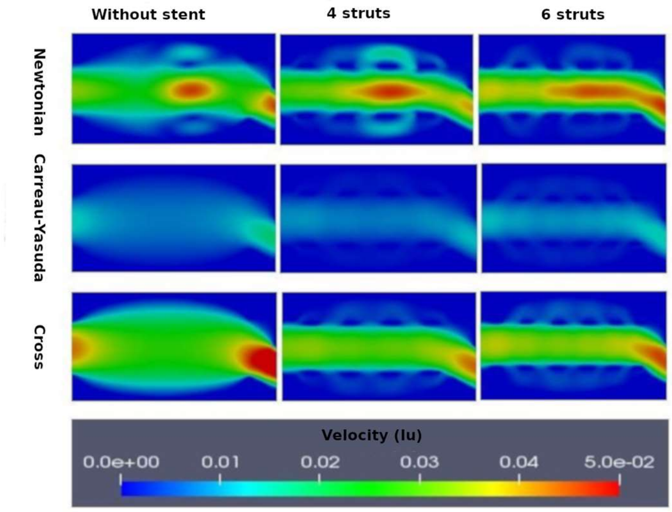

Fig. 12: Representation of the velocity field with different porosities for the three rheological models (diastolic velocity).

Table. V

Maximum velocity values obtained in the control line (inside the sacs) for the three rheological models.

	0 stent	4 struts	6 struts
Newt	0.00189	0.00107	0.00068
C-Y	0.00091	0.00056	0.00042
Cross	0.00174	0.00102	0.00056

Newtonian model

The maximum velocity is around 0.00189 (lu) for a without stent aneurysm, it decreases afterwards to 0.00107 (lu) in the model with four struts and also decreases to reach the value 0.0006 (lu) for the model with six struts. This is due to the decrease in porosity caused by the stent struts at the entrance to the aneurysm.

Carreau-Yasuda model

This model is different from the other two models, the only thing that is similar is that we have a velocity reduction obtained inside the aneurysmal sacs after the placement of a stent. The maximum velocity in the control line inside the sacs decreases from 0.00091 (lu) in the without stent model to 0.00042 (lu) in the six-strut model.

Cross model

Same interpretation as that on the Newtonian model is made. Velocity decreases in aneurysmal sacs after placement of a stent in the aneurysm. The maximum velocity for this model decreases from 0.00174 (lu) for the aneurysm without stent until reaching a value of 0.00056 (lu) in the aneurysm with six struts. These values are smaller than those recorded in the Newtonian model.

Velocity in the middle of the artery

To see the influence of the location of the stents on the flow, we checked the velocities in the middle of the artery for the three rheological models. Table. VI gives the maximum values of velocity (lu) obtained in the middle of the stent.

Table. VI

Maximum velocity values (lu) obtained in the middle of the stent for the three rheological models

	0 stent	4 struts	6 struts
Newt	0.00910	0.01020	0.01080
C-Y	0.00199	0.00210	0.00220
Cross	0.00840	0.00980	0.01020

Upon visualization of the flow of the three models with and without a stent, we notice a considerable increase in the velocity of the flow after the placement of a stent, more precisely in the middle of the stent. This means that the placement of the stent promotes flow towards the exit of the fusiform aneurysm.

3. Shear rate: systolic

Fig. 13 show a presentation of the shear rate between the different models with and without stent in the case of systolic velocity.

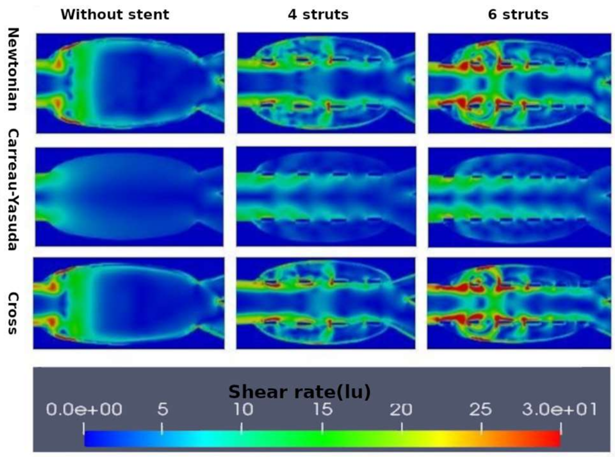

Fig. 13: Representation of the shear rate for the three rheological models (systolic velocity).

The Table. VII below contains the maximum values of the shear rate in the sac of the aneurysm for the three rheological models and for the systolic velocity.

Table. VII

Maximum values of the shear rate (lu) obtained in the sac of the aneurysm for the three rheological models (systolic velocity).

	0 stent	4 struts	6 struts
Newt	24.780	20.410	15.330
C-Y	19.835	16.224	12.187
Cross	24.499	19.246	15.124

Newtonian model

The shear stress values in the parent vessel are greater than the values inside. An increase in shear stress is observed after placement of the stent. The maximum shear stress in the control line is 24.78 (lu) for the model without a stent and increases until reaching a value of 15.33 after the placement of a stent with six struts. This model is different compared with other models. This model gives small values of shear stress inside the aneurysmal sac compared to other models. Its maximum shear stress is 19.835 (lu) for the non-stent model and 12.187 (lu) for the six struts model.

Cross model

This model provides almost the same results as those of the Newtonian model; there is a decrease in shear stress inside the aneurysmal sac after the placement of a stent is observed. The decrease is from 24.499 (lu) for the non-stent model down to 15.124 (lu) for the six-strut model.

4. Shear rate: diastolic

Fig. 14 gives the representation of the shear rate for the three rheological models for the smallest velocity in the abdominal aorta. The Table. VIII below gives the maximum values of the shear rate in the aneurysmal sacs for the three rheological models and for the diastolic velocity.

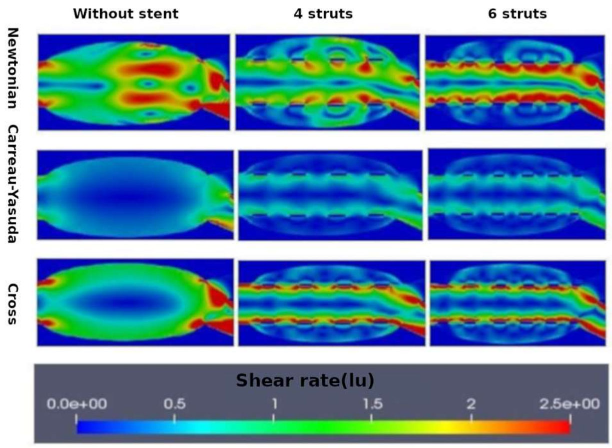

Fig. 14: Representation of the shear rate for the three rheological models (diastolic velocity)

Table. VIII

Maximum values of the shear rate (lu) obtained in the sacs of the aneurysm for the three rheological models (diastolic velocity).

	0 stent	4 struts	6 struts
Newt	1.610	1.140	0.980
C-Y	0.920	0.690	0.650
Cross	1.399	0.920	0.870

Newtonian model

The values of shear stress in the parent vessel are greater than the values inside. Following stent placement, there is an increase in shear stress. The maximum shear stress in the control line is 1.61 (lu) in the absence of a stent and increases to 1.02 after the placement of a six strut stent.

Carreau-Yasuda Model

This model is different compared to the other models as for all the previous visualizations on the velocity fields. This model gives small values of the shear stress inside the aneurysmal sac compared to the other models. The maximum shear stress is 1.12 (lu) for the non-stent model and 0.76 (lu) for the six strut model.

Cross model

This model provides almost the same results as the Newtonian model. An increase in shear stress is observed within the aneurysmal sac after placement of a stent. The increase is from 1.499 (lu) for the aneurysm without stent up to 0.94 (lu) for the stent with six struts.

C. *Quantitative analysis*

To perform a quantitative analysis on the percent change in velocity and shear rate related to stent effect and efficiency, the velocities for the largest and smallest heartbeats were taken to test the role of the stent in different blood flow regimes. To do this analysis, we must look for:

- The rate of change of velocity for the largest heartbeat V_{rg},
- The rate of change of velocity for the smallest heartbeat V_{rp},
- The rate of change in shear rate for the largest heartbeat Tc_{rg}
- The rate of change of the shear rate for the smallest heartbeat Tc_{rp}.

Such as :

$$V_r = \frac{V^{ns} - V^s}{V^{ns}} \times 100$$

$$Tc_r = \frac{Tc^{ns} - Tc^s}{Tc^{ns}} \times 100$$

With, V^s: the velocity for an aneurysm with stent, V^{ns}: the velocity for an aneurysm studied without stent,
Tc^{ns}: the shear rate for an aneurysm without stent and Tc^s: the shear rate for an aneurysm with stent.

Percentage changes in velocity and shear rate are calculated at different points in the aneurysm to see the impact of the stent on blood flow in different parts of the aneurysm. This quantitative analysis on the aneurysm is carried out in order to know the role and the effectiveness of stents.
The quantitative analysis is made for three points of the fusiform aneurysm (at the entrance, in the middle and at the exit of the aneurysm).

1. In the entrance of aneurysmal sac

Model	stent	Porosity (%)	V_{rg} (%)	V_{rp} (%)	Tc_{rg} (%)	Tc_{rp} (%)
Newt	0 stent	100.00	0.00	0.00	0.00	0.00
	4 struts	70.00	5.61	12.30	6.61	4.46
	6 struts	59.00	10.29	18.01	11.18	8.93
C-Y	0 stent	100.00	0.00	0.00	0.00	0.00
	4 struts	70.00	16.95	11.20	18.66	10.90
	6 struts	59.00	20.08	13.79	21.82	16.00
Cross	0 stent	100.00	0.00	0.00	0.00	0.00
	4 struts	70.00	7.77	2.54	5.52	17.36
	6 struts	59.00	12.03	9.60	10.48	22.40

2. In the output of aneurysmal sac

Model	stent	Porosity (%)	V_{rg} (%)	V_{rp} (%)	Tc_{rg} (%)	Tc_{rp} (%)
Newt	0 stent	100.00	0.00	0.00	0.00	0.00
	4 struts	70.00	11.57	8.30	17.57	9.91
	6 struts	59.00	16.80	8.00	22.50	14.69
C-Y	0 stent	100.00	0.00	0.00	0.00	0.00
	4 struts	70.00	5.26	4.58	9.13	6.19
	6 struts	59.00	7.63	6.66	25.82	17.85
Cross	0 stent	100.00	0.00	0.00	0.00	0.00
	4 struts	70.00	17.50	11.38	5.11	2.8
	6 struts	59.00	10.89	14.02	6.92	5.31

3. In the middle of the aneurysmal sac

Model	stent	Porosity (%)	V_{rg} (%)	V_{rp} (%)	Tc_{rg} (%)	Tc_{rp} (%)
Newt	0 stent	100.00	0.00	0.00	0.00	0.00
	4 struts	70.00	5.78	36.36	13.22	14.44
	6 struts	59.00	10.93	19.09	19.09	18.88
C-Y	0 stent	100.00	0.00	0.00	0.00	0.00
	4 struts	70.00	6.25	37.93	25.00	16.25
	6 struts	59.00	8.12	46.89	31.90	20.18
Cross	0 stent	100.00	0.00	0.00	0.00	0.00
	4 struts	70.00	2.08	25.31	29.16	25.81
	6 struts	59.00	3.14	26.46	33.54	38.36

It's noted that there a reduction in the flow velocity and the shear rate in the aneurysmal sacs after the placement of a stent and that it differs from one point to another, and it's also noted a slight increase at the entrance and exit of the aneurysm. The percentage changes in velocity and shear rate are not influenced by the type of pulsation or by the rheological model, but the number of struts (or porosity) influences the results for the three models, where we see that the rate of change for the cases of the stents with six struts is higher than that with four struts, except for a few cases. These results are comparable to the results obtained by [7].
The reduction in hemodynamics obtained remains modest, with a maximum of 40%, which remains probably unfavorable for thrombotic occlusion. The use of multiple overlapping stents is recommended to produce occlusion [7, 21].

II. CONCLUSION

In this work, a numerical investigation was conducted by the Lattice Boltzmann method using a D2Q9 discretization and three types of boundary conditions: bounce-back at the walls; Dirichlet at the entrance; Von Neumann at the exit of our computer code; and visualization on the ParaView software using a pulsed flow.
The results show many sub-cases such as several stents, systolic and diastolic velocity, velocity and shear rate. It is interesting to demonstrate the reduction effect of the stents for each case and for each variable (velocity and shear rate). This detail may seem repetitive but it provides information of a different nature concerning the effect of the stent for the treatment of AAA. Indeed, velocity alone is not enough as an index for monitoring the generation of thrombosis. The shear rate must be added since this index is proposed as a key variable for the appearance and development of thrombosis [22-24].
According to the results found on the case study of the fusiform abdominal aortic aneurysm, it's noted that:

- For all three rheological models, the velocity decreases after the placement of a stent. The decrease in velocity and shear rate for the fusiform aortic aneurysm observed is less significant compared to the case of the saccular intracranial aneurysm. This explains the formation of thrombosis for cerebral aneurysms compared to abdominal aortic aneurysms.
- The velocity field results given by the Carreau-Yasuda model are different compared to the other two models, and the Newtonian model presents the greatest velocity values for the two cases of aneurysms treated.
- The velocity values for the Newtonian and Cross models are very close.
- For all three rheological models, the velocity increases in the middle of the fusiform aneurysm after the placement of a stent. The decrease in the porosity of the stents slows the flow in the aneurysmal sacs and increases the flow in the middle of the artery.
- The effect of stents is more clearly visualized in the case of systolic velocity than in the case of diastolic velocity.
- The shear rate values are much higher in the case of the abdominal aortic aneurysm than in the anterior cerebral aneurysm, which coincides with the medical theory that the phenomenon of thrombosis is rare in aortic aneurysms (a high value of the shear rate indicates a low probability of thrombosis formation [23]).
- The purpose of placing stents in the case of cerebral saccular aneurysms is to promote the formation of thrombosis inside the aneurysmal sac. The purpose of placement of stents in the case of abdominal aortic aneurysm is to promote blood flow to the outside of the aneurysm in the case of abdominal aortic aneurysm and to decrease the pressure on the aneurysmal sac.
- The effect of stents is more visualized in the case of systolic velocity than diastolic velocity.
- The increase in flow velocity entering and exiting the fusiform aneurysm is much greater than that of the saccular aneurysm after stent placement, confirming that the stent is usable to promote horizontal flow in the case of fusiform aneurysms. However, if a thrombotic occlusion is desired, several stents must be superimposed.
- The pulsation of the heart has no influence on the quantitative analysis of the flow.

The main obstacle to the development of this work is the lack of relevant experimental studies in order to validate the findings given by numerical simulations.

REFERENCES

[1] Mrabet, H.E., I. Mlouki, S. Nouira, O. Hmaied, A. Ben Abdelaziz, and S. El Mhamdi, Cardiovascular risk factors in the Maghreb. A systematic review. Tunis Med, 2021. 99(1): p. 120-128.

[2] Nieuwkamp, D., L. Setz, A. Algra, F. Linn, N. de Rooij, and G. Rinkel, Changes in case fatality of aneurysmal subarachnoid haemorrhage over time, according to age, sex, and region: a meta-analysis. Lancet Neurol, 2009. 8(7): p. 635-642. DOI: 10.1016/S1474-4422(09)70126-7

[3] Andersson, M., M. Talvitie, L. Benson, J. Roy, H. Roos, and R. Hultgren, A population-based study of post-endovascular aortic repair rupture during 15 years. J Vasc Surg, 2021. 74(3): p. 701-710.e3.

[4] Toth, G. and R. Cerejo, Intracranial aneurysms: Review of current science and management. Vasc Med, 2018. 23(3): p. 276-288.

[5] InformedHealth.org [Internet]. Cologne, G.I.f.Q.a.E.i.H.C.I., When is surgery recommended for the treatment of abdominal aortic aneurysm? 2017 Jun 14.

[6] Sfyroeras, G.S., I. Dalainas, T.G. Giannakopoulos, K. Antonopoulos, J.D. Kakisis, and C.D. Liapis, Flow-diverting stents for the treatment of arterial aneurysms. J Vasc Surg, 2012. 56(3): p. 839-46.

[7] Wang, S., Y. Zhang, J. Feng, Y. Huang, P. Hui, J.H. Gillard, . . . Z. Teng, The role of porosity and 3D cross-stent configuration of multiple overlapping uncovered stents in the management of complex aortic aneurysms – Insights from haemodynamics. Medicine in Novel Technology and Devices, 2019. 3: p. 100020.

[8] Mohamad, A.A., Lattice Boltzmann Method. Fundamentals and Engineering Applications with Computer Codes. 2019: Springer London.

[9] Krüger, T., H. Kusumaatmaja, A. Kuzmin, O. Shardt, G. Silva, and E.M. Viggen, The Lattice Boltzmann Method. Principles and Practice. Graduate Texts in Physics. 2017: Springer, Cham. XXIV, 694.

[10] Sukop, M.C. and D.T. Thorne, Lattice Boltzmann Modeling: An Introduction for Geoscientists and Engineers. 2006: Springer.

[11] Chopard, B. and M. Droz, Cellular Automata Modeling of Physical Systems. 1998: Cambridge University Press.

[12] Dupuis, A., From a Lattice Boltzmann model to a parallel and reusable implementation of a virtual river. 2002, University of Geneva: Switzerland.

[13] Zou, Q. and X. He, On pressure and velocity boundary conditions for the lattice Boltzmann BGK model. Physics of fluids, 1997. 9(6): p. 1591-1598.

[14] Walther, E., Contribution de la Lattice Boltzmann Method `a l'´etude de l'enveloppe du bâtiment. 2016, Université Paris-Saclay.

[15] Cheng, T. and D. Michel, Pulsatile flow of non-newtonian fluids through arterial stenoses. J. Biomechanics, 1996. 29(7): p. 899-908.

[16] Siobhan, O.C., W. Michael, and M. Timothy, Numerical modelling of Newtonian and non-Newtonian representation of blood in a distal end-to-side vascular bypass graft anastomosis. Medical Engineering & Physics, 2006. 28: p. 70–74.

[17] Safoora, K., D. Mahsa, V. Paritosh, D. Mitra, D. Bahram, and J. Payman, Effect of rheological models on the hemodynamics within human aorta: CFD study on CT image-based geometry. Journal of Non-Newtonian Fluid Mechanics, 2014. 207: p. 42–52.

[18] Torlai, F.G., G.S.P. Meirelles, F. Miranda Jr, J.H.A. da Fonseca, S. Ajzen, and G. D'Ippolito, A proposal for standardizing computed tomography reports on abdominal aortic aneurysms. Radiologia Brasileira, 2006. 39: p. 259-262.

[19] NATIONAL HEART, L., AND BLOOD INSTITUTE. What Is Aortic Aneurysm? [cited 2022 22Sep]; Available from: https://www.nhlbi.nih.gov/health/aortic-aneurysm.

[20] Taylor, C.A., T.J. Hughes, and C.K. Zarins, Finite element modeling of three-dimensional pulsatile flow in the abdominal aorta: relevance to atherosclerosis. Ann Biomed Eng, 1998. 26(6): p. 975-87.

[21] Yeow, S.L. and H.L. Leo, Is Multiple Overlapping Uncovered Stents Technique Suitable for Aortic Aneurysm Repair? Artif Organs, 2018. 42(2): p. 174-183. DOI: 10.1111/aor.12993

[22] Mezali, F., K. Naima, S. Benmamar, and A. Liazid, Study and modeling of the thrombosis of small cerebral aneurysms, with and without flow diverter, by the lattice Boltzmann method. Computer Methods and Programs in Biomedicine, 2023. 233: p. 107456.

[23] Mezali, F., S. Benmamar, K. Naima, H. Ameur, and O. Rafik, Evaluation of stent effect and thrombosis generation with different blood rheology on an intracranial aneurysm by the Lattice Boltzmann method. Computer Methods and Programs in Biomedicine, 2022. 219: p. 106757.

[24] Chopard, B., R. Ouared, D.A. Ruefenacht, and Y. Hasan, Lattice Boltzmann Modeling of Thrombosis in Giant Aneurysms. INTERNATIONAL JOURNAL OF MODERN PHYSICS C, 2007. 18(4): p. 712-721. DOI:10.1016/j.matcom.2006.05.025

Farouk Mezali was born in Thénia, Algeria, in 1980. He received the Engineer's degrees in Hydraulic Engineering from Ecole Nationale Polytechnique (ENP) of Algiers in 2003, the Magister degree from Ecole Nationale Polytechnique, Algiers, in 2006. He is currently a Ph.D. student at the Hydraulic Department at the same Engineering School and assistant professor at Mohamed Boudiaf University of M'sila**.**

Saâdia Benmamar is a professor at Ecole Nationale Polytechnique. She was the head of hydraulic engineering department. Currently, she is the director of the of the LRS-EAU laboratory in same Engineering School. His current research interests include CFD, open channel flow, and hydrology.

Mohamed Saber Hamouda in 2019, he obtained a degree in hydraulic engineering from the National Polytechnic School of Algiers. Currently, he is a supervisor at the Elhamma desalination plant at Suez WTS.Mohamed.

Aghiles Zakaria Mezali obtained a degree in hydraulic engineering in 2019, from the National Polytechnic School of Algiers. He is currently an operation engineer at SEAAL (Société des Eaux et de l'Assainissement d'Alger).